Polymer Chemistry

Effect of Halogen and Solvent on Iron-Catalyzed Atom Transfer Radical Polymerization

Journal:	*Polymer Chemistry*
Manuscript ID	PY-ART-12-2021-001601.R1
Article Type:	Paper
Date Submitted by the Author:	04-Jan-2022
Complete List of Authors:	Dadashi-Silab, Sajjad; Carnegie Mellon University, Department of Chemistry Kim, Khidong ; Carnegie Mellon University, Department of Chemistry Lorandi, Francesca; University of Padova Department Industrial Engineering, Industrial Engineering Schild, Dirk; Carnegie Mellon University, Department of Chemistry Fantin, Marco; Carnegie Mellon University, Department of Chemistry Matyjaszewski, Krzysztof; Carnegie Mellon University, Department of Chemistry

ARTICLE

Effect of Halogen and Solvent on Iron-Catalyzed Atom Transfer Radical Polymerization

Received 00th January 20xx,
Accepted 00th January 20xx

DOI: 10.1039/x0xx00000x

Sajjad Dadashi-Silab,† Khidong Kim,† Francesca Lorandi, Dirk J. Schild, Marco Fantin, and Krzysztof Matyjaszewski*

Efficient transfer of halogen atoms is essential for controlling the growth of polymers in atom transfer radical polymerization (ATRP). The nature of halogens may influence the efficiency of the halogen atom transfer during the activation and deactivation processes. The effect of halogens can be associated with the C-X bond dissociation energy and the affinity of the halogens/halides to the transition metal catalyst. In this paper, we study the effect of halogens (Br *vs.* Cl) and reaction media in iron-catalyzed ATRP in the presence of halide anions as ligands. In Br-based initiating systems, polymerization of methacrylate monomers was well-controlled whereas Cl-based initiating systems provided limited control over the polymerization. The high affinity of the Cl atom to the iron catalyst renders it less efficient for fast deactivation of growing chains, resulting in polymers with molecular weights higher than predetermined by $\Delta[M]/[RX]_o$ and with high dispersities. Conversely, Br can be exchanged with higher efficiency and hence provided good control over polymerization. Decreasing the polarity of the reaction medium improved the polymerization control. Polymerizations using ppm levels of the iron catalyst in acetonitrile (a more polar solvent) yielded polymers with larger dispersity values due to the slow rate of deactivation as opposed to the less polar solvent anisole, which afforded well-controlled polymers with dispersity <1.2.

Introduction

The development of reversible deactivation radical polymerization (RDRP) techniques has revolutionized the synthesis of well-defined polymers.[1, 2] RDRP methods offer precise control over molecular weight and dispersity, composition, and architecture of the polymers. Most common RDRP methods include atom transfer radical polymerization (ATRP),[3-5] reversible addition-fragmentation chain transfer,[6, 7] and nitroxide-mediated polymerizations.[8] While these techniques differ in their underlying mechanisms, a common feature of all RDRPs is to reduce the fraction of terminated chains among the large pool of dormant species and provide rapid dynamic exchange between them via reversible deactivation processes.

In ATRP, catalysts are employed to provide control over the growth of polymer chains. ATRP catalysis is a redox process that involves the reversible transfer of halogen atoms through activation of dormant polymer chains by the lower oxidation state catalyst (activator, L/Mt^n) as well as deactivation of the growing radicals by the higher oxidation state catalyst bonded to a halogen atom (deactivator, L/Mt^{n+1}-X).[9] Therefore, the efficiency of the halogen atom transfer in both activation and deactivation steps is essential for promoting polymerization and gaining control in ATRP.

Activation of halogen-capped chain ends depends on dissociation energy of the C-X bond as well as the halogenophilicity of the catalyst, which defines its ability to abstract a halogen atom and the affinity of the latter to the catalyst. For different halogens, C-X bond dissociation energy changes in the order F > Br > Cl > I, with the C-F bond being so strong that renders activation slow and inefficient.[10] On the other hand, for copper based systems, the catalyst-halogen bond (L/Mt^{n+1}-X) becomes stronger moving from I to F. Therefore, because of the low affinity of the catalyst to iodine and high bond dissociation energy of the C-F bond, metal-catalyzed ATRP with I and F functionalities is less successful.[11] Although polymerizations in the presence of alkyl iodides using Cu complexes can be challenging, the I functionality can be used in conjunction with iodide salts,[12, 13] amines,[13] or some iron complexes[14, 15] to catalyze well-controlled polymerizations which may also proceed through a degenerative transfer process.[16]

The strong bond between the catalyst and halogen atom in the deactivator (L/Mt^{n+1}-X) may hamper fast deactivation of propagating chains and therefore result in polymers with higher dispersity. For example, because of the strong bond between Cl and the catalysts commonly employed in ATRP, Cl-based ATRP systems typically show slower deactivation and result in polymers with relatively larger dispersity.[17] Thus, Br is the most reactive chain end functionality in ATRP that balances the opposing factors of bond dissociation energy of C-X and catalyst

[a] *Department of Chemistry, Carnegie Mellon University, 4400 Fifth Avenue, Pittsburgh, Pennsylvania 15213, United States.*
**Email: matyjaszewski@cmu.edu*
† These authors contributed equally to this work.
Electronic Supplementary Information (ESI) available: [details of any supplementary information available should be included here]. See DOI: 10.1039/x0xx00000x

halogenophilicity, hence provides fast and well-controlled ATRP.

In this paper, we aim to study the influence of halogen nature in iron-catalyzed ATRP in the presence of halide anions as ligands. Iron-based complexes form an important class of ATRP catalysts.[18-20] Research in iron catalysis has been focused on developing new efficient ligand families that can provide control over polymerizations. Ligands such as nitrogen[21, 22] or phosphorus-containing compounds,[23-29] imines,[30-33] amine-bis(phenolate)s[34-36] and salts with halide anions[37-46] are among the widely used ligands in iron-catalyzed ATRP. Halide salts form anionic iron species that have higher catalytic activity in ATRP than their neutral or cationic counterparts. Polar solvents may also promote formation of cationic iron species that do not participate in catalysis. In addition, the high stability of anionic iron species in polar media may lead to a slow deactivation of the growing chains and thus requiring high concentrations of the catalyst to provide well-controlled polymerizations.[41] Accordingly, control in low ppm (ppm: parts per million) iron-catalyzed ATRP may be compromised in polar media.

Despite the breadth of research in developing diverse ligand families for iron-catalyzed ATRP, the effect of halogens and reaction media on polymerization control has not been fully explored in these systems. Here, we study these parameters in ATRP using low concentration of iron halides in the presence of halide anions that serve as ligands. We show that the high affinity of Cl to Fe resulted in lower deactivation efficiency and therefore limited control over polymerization of methacrylate monomers. However, Br-based initiating systems in anisole yielded well-defined polymers with low dispersities.

Results and discussion

UV-Vis studies

We began our studies by spectroscopic analysis of the iron catalysts using UV-Vis spectroscopy or cyclic voltammetry (CV) in the presence of both Br and Cl anions. In the UV-Vis experiments, solutions of $FeBr_3$ or $FeCl_3$ in anisole or acetonitrile (MeCN) were titrated by addition of tetrabutylammonium bromide (TBABr) or tetrabutylammonium chloride (TBACl) salts. In the absence of additional halide salts, both $FeBr_3$ and $FeCl_3$ formed neutral species in anisole as this apolar solvent does not favor disproportionation/dismutation and/or formation of ionic species (Figure 1). The observed spectra of $FeBr_3$ and $FeCl_3$ have single maximum (300-400 nm range) in anisole, similar to that of $FeCl_3$ reported in tetrahydrofuran or in the gas phase.[47, 48] Addition of halide salts resulted in a change in the UV-Vis spectra of $FeCl_3$ as two absorbance maxima appeared, indicating formation of anionic FeX_4^- species. $FeCl_3$ showed absorption mainly in the UV region below 400 nm, whereas $FeBr_3$ absorbed in the visible region > 550 nm. Addition of TBACl to $FeCl_3$ resulted in the formation of two absorbance peaks, whereas in the presence of TBABr added to $FeCl_3$, the spectra showed a tailing toward higher wavelengths (Figure 1-A and B) but still contained the same peak maxima, as observed in Figure 1-A. This absorption spectra can be associated with the

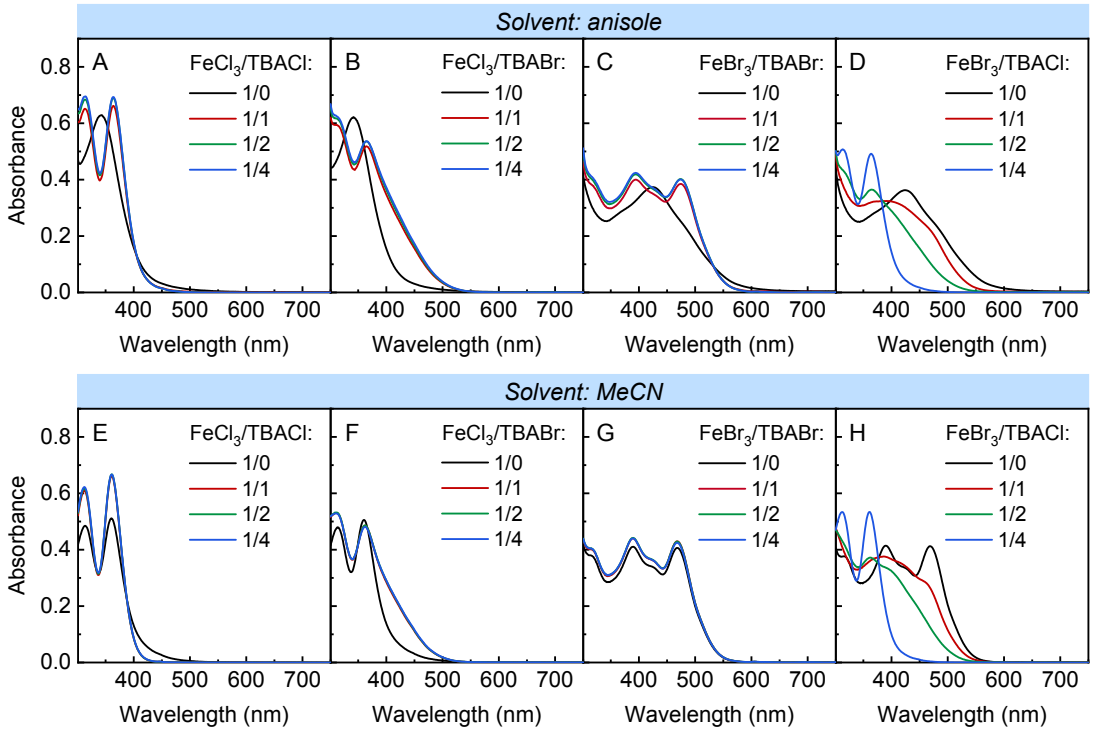

Figure 1. UV-Vis spectra of iron species with halide salts as ligands in anisole (top) or MeCN (bottom). (A) and (E) $FeCl_3$ + TBACl, (B) and (F) $FeCl_3$ + TBABr, (C) and (G) $FeBr_3$ + TBABr, and (D) and (H) $FeBr_3$ + TBACl. [FeX_3] = 0.1 mM, [TBAX] = 0, 0.1, 0.2, and 0.4 mM. The absorptions with one maximum (in anisole) correspond to the FeX_3 species whereas those with two maxima correspond to the anionic species, FeX_4^-.

formation of $FeBrCl_3^-$. Further increase of TBABr concentration did not change the absorption spectra indicating that Cl preferably binds to Fe over Br. Upon addition of TBABr to $FeBr_3$, its absorption changed with two main peaks appearing at > 400 nm, attributed to the formation of the anionic $FeBr_4^-$ species (Figure 1-C).

Interestingly, Figure 1-B did not show an absorption maximum at ~470 nm, suggesting that no FeBr4$^-$ was formed even upon addition of 4 equiv. of TBABr to FeCl3. Thus, even with a large excess of TBABr with respect to $FeCl_3$, $FeBrCl_3^-$ was the predominant species. In contrast, addition of TBACl to the solution of $FeBr_3$ significantly changed the UV-Vis spectra with a blue shift that further changed as the concentration of TBACl was increased (Figure 1-D). In the presence of 4 equiv. of TBACl with respect to $FeBr_3$, the spectrum was similar to those obtained with $FeCl_3$/TBACl (Figure 1-A), indicating replacement of all Br with Cl and formation of $FeCl_4^-$. No change was observed upon further addition of TBACl. These observations confirm the higher affinity of the Cl atom *vs.* Br to bind to Fe, which may consequently affect the deactivation of growing chains because of the formation of a strong Fe-Cl bond.

In MeCN, the UV-Vis spectra of $FeCl_3$ or $FeBr_3$ showed two absorption peaks which can be attributed to the formation of anionic iron species in the absence of any additional halide salt ligands (Figure 1-E and G, respectively). Polar solvents such as MeCN can stabilize/promote formation of the anionic and cationic iron species via disproportionation or ligand displacement by the solvent molecules. Addition of TBABr to $FeCl_3$, slightly changed the spectra with a tailing toward higher wavelengths (Figure 1-F). Furthermore, upon addition of TBACl to a solution of $FeBr_3$ in MeCN, the UV-Vis spectra gradually blue-shifted (~100 nm) to finally resemble that of $FeCl_3$/TBACl in the presence of 4 equiv. of TBACl (Figure 1-H).

Electrochemical analysis

Electrochemical analysis of the iron catalysts using cyclic voltammetry provided further insight into the interaction of Fe with Br and Cl anions. Because of the polarity of anisole, the CV measurements were performed only in MeCN by titration of both $FeBr_3$ and $FeCl_3$ with Br or Cl anions (Figure 2). The CV spectrum of $FeCl_3$ (in the absence of additional anions) showed that the main reduction peak was preceded by a pre-peak, indicating the presence of at least two Fe^{III} species in the solution (Figure 2-A). Similarly, the oxidation signals were broad and showed two main oxidation peaks. This complex redox pattern suggests the formation of multiple iron species once $FeCl_3$ is solvated, such as $FeCl_2^+$, $FeCl_3$, and $FeCl_4^-$ (additional solvent molecules that may be present in the coordination sphere are omitted for simplicity).

Upon progressive addition of TBACl (1-4 equiv.), the voltametric pattern simplified; the peak couples at more positive potentials disappeared, while the peak couple at more negative potentials substantially increased in intensity. In agreement with the UV-Vis experiments, the peak couple at more negative potentials was attributed to the reversible redox couple of $Fe^{III}Cl_4^-/Fe^{II}Cl_4^{2-}$ with half-wave potential of $E_{1/2}$ = +0.02 V vs. saturated calomel electrode, SCE.

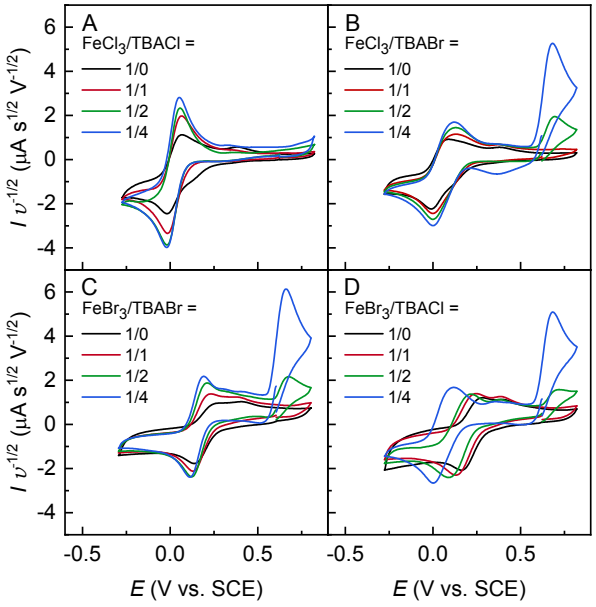

Figure 2. Cyclic voltammetry of iron species in the presence of different amounts of TBABr or TBACl in MeCN at a scan rate of 100 mV/s. [FeX_3] = 1 mM, $TEABF_4$ (0.1 M) as a supporting electrolyte.

Titration of $FeCl_3$ with one and two equiv. of Br anion shifted the main cathodic peak only slightly to more positive potentials while the main anodic peak shifted > 30 mV to more positive values due to substitution of MeCN with Br anion (Figure 2-B). This observation indicates that Br anions are more competitive with Cl anions in binding to Fe^{II} than Fe^{III} species. Further addition of TBABr only resulted in the appearance and progressive increase of the irreversible oxidation peak corresponding to free Br^- (~0.75 V vs SCE). Thus, additional Br^- did not significantly affect the coordination environment of Fe species.

For $FeBr_3$, both in the absence or presence of 1 equiv. of TBABr, a broad reduction peak was observed (Figure 2-C). The addition of TBABr narrowed the reduction peak that shifted ~15 mV to more negative values (Figure 2-C). Two oxidation peaks were present (at ~0.27 and ~0.42 V vs SCE) in the absence of TBABr, and their relative intensities were only slightly affected by the addition of 1 equiv. of TBABr. Overall, the behavior is similar to $FeCl_3$ with $Fe^{III}Br_4^-$ being the dominant Fe^{III} species. For Fe^{II} species, the speciation is more complicated. Upon addition of 2 equiv. of TBABr, the relative intensity of the oxidation peak at ~0.42 V vs SCE decreased, however another oxidation peak at ~0.75 V vs SCE appeared, which is ascribed to the oxidation of free Br anions. Therefore, additional Br anions did not coordinate to the complex.

Titration of $FeBr_3$ with Cl anions showed a gradual change in the CV signal of the complex to finally resemble that of $FeCl_3$/TBACl in the presence of 4 equiv. of TBACl. Addition of 1 equiv. of TBACl to a solution of $FeBr_3$ in MeCN shifted both the cathodic and anodic peak to more negative potentials. When 2 equiv. of TBACl were added, the peak corresponding to the oxidation of free Br anions appeared and increased in intensity with increasing the amount of TBACl. This observation indicates that

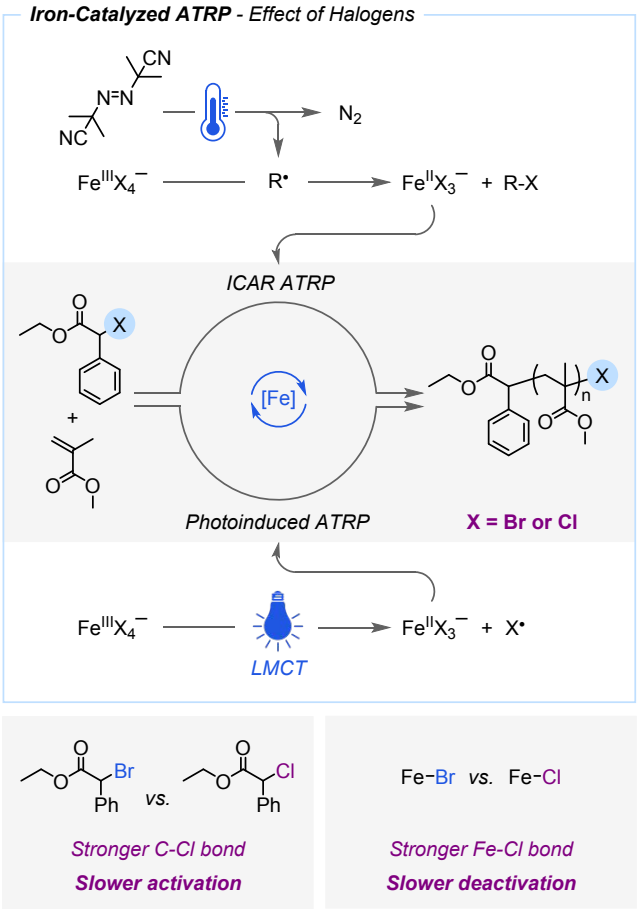

Scheme 1. Iron-catalyzed ATRP under ICAR or photoinduced ATRP conditions (LMCT: ligand-to-metal charge transfer). Effect of halogens (X: Br vs. Cl) can be related to both the activation and deactivation processes by the iron catalyst.

Br anions are progressively displaced by Cl anions, which bind more strongly to Fe species.

Polymerizations

The spectroscopic analyses of the iron catalysts indicate that Cl binds more strongly to Fe compared to Br, and therefore may affect the deactivation process and control over polymerization.

To investigate the effect of halogen in iron-catalyzed ATRP, polymerization reactions were performed under ICAR (initiators for continuous activator regeneration) or photoinduced ATRP conditions in the presence of different halides in both the initiator and the catalyst (Scheme 1).

ICAR ATRP of methyl methacrylate (MMA) was performed using azobisisobutyronitrile (AIBN) as a radical source and Br or Cl-based initiators and catalysts. The Br-based initiating system used ethyl α-bromophenylacetate (EBPA) as the initiator and $FeBr_3$/TBABr as the catalyst (4 mol% with respect to EBPA, i.e., 400 ppm *vs.* MMA). In the absence of additional TBABr, polymerization of MMA in anisole provided low monomer conversion (Entry 1, Table 1). The importance of TBABr in affording a highly active iron catalyst was shown in ATRP of MMA with the $FeBr_3$/TBABr catalyst (1/1 ratio) that yielded high monomer conversion (95%) and a polymer with controlled molecular weight and low dispersity of 1.16 (Entry 2, Table 1). Using MeCN as a solvent under the same conditions, the polymers showed a higher dispersity > 1.6 in the presence or absence of additional TBABr (Entries 3 and 4, Table 1). Further increasing the ratio of TBABr from 1 to 4 (with respect to Fe) did not improve control (Entry 5, Table 1). Thus, a polar medium may diminish deactivation rate, especially when using low concentration of catalyst, in contrast to high catalyst concentration systems.[49]

The effect of MeCN in iron-catalyzed ATRP was further demonstrated by performing the UV-Vis analysis of the catalyst and polymerization of MMA with varying ratios of anisole and MeCN as solvents. Addition of MeCN to a solution of $FeBr_3$ in anisole resulted in a progressive change in the UV-Vis spectra of the solution showing absorption peaks at ~390 and ~470 nm that resembled formation of the anionic iron species upon addition of MeCN (1-10 vol% with respect to anisole) (Figure S6). In polymerization, ICAR ATRP of MMA in 100% anisole afforded well-controlled polymers using the Br-based initiating system. Increasing the volume ratio of MeCN with respect to anisole (from 0 to 25, 50, 75, and 100 vol%), showed an increase in the dispersity of the resulting polymers, while experimental molecular weights agreed well with theoretical values. For

Table 1. Results of iron-catalyzed ICAR ATRP of MMA with different halides [a]

Entry	R-X	Catalyst	Solvent	Conv. (%)	$M_{n,th}$	M_n	$Đ$
1	EBPA	$FeBr_3/Br^-$ (1/0)	Anisole	33	3500	3600	1.34
2	EBPA	$FeBr_3/Br^-$ (1/1)	Anisole	95	9700	9000	1.16
3	EBPA	$FeBr_3/Br^-$ (1/0)	MeCN	79	8200	5600	1.67
4	EBPA	$FeBr_3/Br^-$ (1/1)	MeCN	90	9300	8700	1.68
5	EBPA	$FeBr_3/Br^-$ (1/4)	MeCN	90	9300	9700	1.60
6	EBPA	$FeCl_3/Cl^-$ (1/1)	Anisole	91	9450	8700	1.19
7	ECPA	$FeBr_3/Br^-$ (1/1)	Anisole	94	9750	10300	1.68
8	ECPA	$FeCl_3/Cl^-$ (1/1)	Anisole	97	10000	12800	1.70
9	ECPA	$FeCl_3/Cl^-$ (1/1)	MeCN	96	9900	16200	1.94
10	ECPA	$FeCl_3/Cl^-$ (1/4)	MeCN	92	9600	22000	1.95

[a] Reaction conditions: [MMA]/[EXPA]/[FeX_3]/[TBAX]/[AIBN] = 100/1/0.04/0.04/0.4 (X = Br or Cl) in 50 vol% solvent at 65 °C for 18 h.

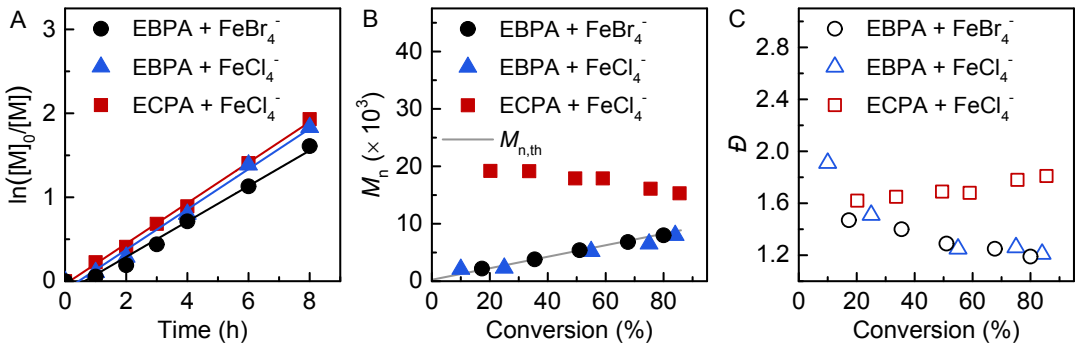

Figure 3. (A) Kinetics and evolution of (B) molecular weight (M_n) and (C) dispersity ($Đ$) in iron-catalyzed ATRP with Br or Cl-based initiating systems. Reaction conditions: [MMA]/[EXPA]/[FeX_3]/[TBAX]/[AIBN] = 100/1/0.04/0.04/0.4 (X = Br or Cl) in anisole (50 vol%) at 65 °C.

example, in 25 vol% MeCN, the dispersity of the polymers increased from 1.18 to 1.24. Further addition of MeCN in 50 or 75 vol%, afforded polymers with dispersity values of 1.28 and 1.36, respectively. In the presence of 100% MeCN, dispersity of the polymers was 1.69 (Table S2 and Figure S7). The increase in the dispersity of the polymers in iron-catalyzed ATRP of MMA with increasing amounts of MeCN may be attributed to the formation of iron species that have low deactivation efficiencies in ATRP. The high stability of the deactivator $FeBr_4^-$ in a polar solvent such as MeCN might be responsible for its low reactivity and diminished deactivation rate of the growing chains.

Previous works have shown that well-controlled iron-catalyzed ATRP could be achieved in MeCN under either normal[49] or photoinduced[50, 51] ATRP conditions where equimolar ratios of the catalyst were used with respect to the initiator. With the high concentration of the iron catalysts, polymerizations can be well-controlled in MeCN. In contrast, ppm levels of the iron catalyst provide limited control over the polymerization due to the slow rate of deactivation and therefore result in polymers with large dispersity. Furthermore, in a recent study, we showed that ATRP of semi-fluorinated monomers with ppm levels of the iron catalyst could also be controlled in MeCN.[43] Because of the high hydrophobicity of the fluorinated monomers, the overall polarity of the reaction medium containing MeCN was lowered and the deactivation of the growing radicals by $FeBr_4^-$ improved in a less polar medium.

To show the effect of the polarity of reaction medium, ICAR ATRP of a semi-fluorinated monomer, 2,2,2-trifluoroethyl methacrylate (TFEMA), was performed in MeCN. The overall polarity of the reaction medium in a mixture of TFEMA in MeCN was lower as compared to MMA in MeCN. Accordingly, ATRP of TFEMA provided well-controlled polymers with a low dispersity of 1.15 (conversion = 88%, M_n = 12000, Figure S8). These results indicate that the deactivation of growing chains by $FeBr_4^-$ in polar media is not efficient enough to yield polymethacrylates with low dispersity in the presence of ppm levels of the catalyst. Next, the effect of different halides systems (Br vs Cl) was investigated. With $FeCl_3$/TBACl (4 mol%) as the catalyst and EBPA as the initiator in anisole, slightly higher dispersity of 1.22 was obtained compared to $FeBr_3$/TBABr and EBPA (Entry 6 *vs.* 1, Table 2). This observation suggested that introducing Cl^- in the system hampered polymerization control. Indeed, using a Cl-based initiator, ethyl α-chlorophenylacetate (ECPA), in the presence of either $FeBr_3$/TBABr or $FeCl_3$/TBACl polymers with high dispersities were obtained (>1.7), indicating poor control over polymerization with Cl-based initiating systems in iron-catalyzed ATRP (Entries 7 and 8, Table 2). The total ratio Br/Cl was 1/0.16 in entry 6 but 0.16/1 in entry 7, Table 1. Polymerizations conducted with the Cl-based initiating system in MeCN showed even larger dispersity values, suggesting worse deactivation in MeCN compared to anisole in the presence of Cl (Entries 9 and 10, Table 1).

To further demonstrate the effect of Br *vs.* Cl, kinetics of polymerization of MMA under ICAR ATRP conditions was investigated using both Br-, and Cl-based initiating systems in anisole. Both systems showed similar rate of polymerization (Figure 3-A). However, molecular weight analysis of the resulting polymers showed that poor control was obtained over the polymerization of MMA in the Cl-based initiating system (Figure 3-B). The molecular weights were higher than theoretical values and decreased as polymerization progressed. The evolution of molecular weight in the Cl-based initiating system indicates a slow activation of ECPA and slow deactivation of the growing chains in the presence of the $FeCl_4^-$ catalyst (dispersity values ~1.6-1.8, Figure 3-C). The strong Fe-Cl bond resulted in a diminished rate of deactivation and hence provided polymers with large dispersity.[52] In contrast, well-controlled polymerization of MMA was observed in the presence of the Br-based initiating system. Molecular weights increased as a function of monomer conversion in line with theoretical values. Moreover, the resulting polymers showed low dispersity values (< 1.2) suggesting a well-controlled polymerization was obtained in the presence of Br-based initiating system (Figure S10). Furthermore, well-controlled polymerization of MMA was achieved in the presence of Br-based initiating system using 400, 200, and 100 ppm of the iron catalyst with respect to the monomer (Figure S11). Interestingly, when a Br-based initiator, EBPA, was used with $FeCl_4$/TBACl as the catalyst (4 mol%) polymerization of MMA was well-controlled, as observed in the presence of all Br-based initiating system (both EBPA and $FeBr_4^-$). Considering the relative ratio of EBPA and $FeCl_4^-$ (1 to 0.04), Br is present in sufficient amount, resulting in efficient atom transfer and deactivation of the growing chains.

Table 2. Results of iron-catalyzed photoinduced ATRP of MMA with different halides [a]

Entry	R-X	Catalyst	Solvent	Light	Conv. (%)	$M_{n,th}$	M_n	$Đ$
1	EBPA	$FeBr_3/Br^-$ (1/0)	Anisole	Blue	59	6100	10900	2.18
2	EBPA	$FeBr_3/Br^-$ (1/1)	Anisole	Blue	96	9900	11600	1.23
3	EBPA	$FeBr_3/Br^-$ (1/1)	MeCN	Blue	94	9700	9400	1.56
4	EBPA	$FeBr_3/Br^-$ (1/4)	MeCN	Blue	75	7700	8100	1.61
5	ECPA	$FeCl_3/Cl^-$ (1/1)	Anisole	Blue	80	8300	16800	1.75
6	EBPA	$FeBr_3/Br^-$ (1/1)	Anisole	Violet	96	9900	10600	1.20
7	ECPA	$FeCl_3/Cl^-$ (1/1)	Anisole	Violet	95	9800	7300	2.08

[a] Reaction conditions: [MMA]/[EXPA]/[FeX_3]/[TBAX] = 100/1/0.04/0.04 (X = Br or Cl) in 50 vol% solvent (anisole or MeCN) under blue (460 nm, 12 mW/cm^2) or violet (400 nm, 10 mW/cm^2) LEDs for 18 h.

Kinetics of the ICAR ATRP of MMA in MeCN showed high initiation efficiency and controlled molecular weights with high dispersity throughout the polymerization (Figure S12).

Iron-catalyzed ATRP can also be photochemically controlled via generation of the activator L/Fe^{II} under light irradiation (Scheme 1). The Fe- Br bond in L/Fe^{III}-Br can be homolytically cleaved to generate L/Fe^{II} and $Br^•$ radicals via a ligand to metal charge

transfer process. The iron catalyst with Br or Cl anions showed different absorption spectra with $FeBr_3$ absorbing in the visible light region and $FeCl_3$ absorbing at the UV region (below 400 nm). Therefore, photoinduced ATRP using iron catalysts was attempted under both blue (460 nm) and violet (400 nm) LED lights to ensure proper photoexcitation of both species. The results of polymerization of MMA with iron in the presence of different halides are summarized in Table 3. Polymerization of MMA using $FeBr_3$ without additional TBABr ligand showed low monomer conversion and polymers with a large dispersity of 2.18. However, when TBABr was added as a ligand, polymerization of MMA in anisole yielded well-controlled polymers. These results indicate the importance of TBABr as a ligand for obtaining the active iron catalysts. Similar to ICAR ATRP results, Br-based systems resulted in well-controlled polymerizations under both blue and violet lights (Entries 2 and 6, Table 3). However, in the Cl-based system control over polymerization was poor showing polymers with high dispersity (Entries 5 and 7, Table 3).

Block copolymerization experiments were performed to confirm the preserved chain end functionality in the resulting polymers under both ICAR and photoinduced ATRP conditions. A PMMA-Br macroinitiator was first synthesized under ICAR ATRP (M_n = 8700, $Đ$ = 1.13). Chain extension of the PMMA-Br macroinitiator with benzyl methacrylate (BzMA) resulted in formation of the second block, yielding controlled block copolymer with molecular weights shifting to higher values and high blocking efficiency (M_n = 15900, $Đ$ = 1.15, Figure 4-A). Similarly, block co-polymerization was successfully achieved under photoinduced ATRP conditions (Figure 4-B).

Conclusions

In summary, Cl-based initiating systems provided inferior control in iron-catalyzed ATRP in the presence of halide anions as ligands. The high affinity of Cl to iron led to inefficient deactivation of the growing chains and therefore provided poor control over polymerization. In the presence of Br-based initiating systems, well-controlled polymerization of methacrylate monomers was achieved with well-defined molecular weights and low dispersities (< 1.2), as demonstrated in synthesis of homo and block copolymers. Furthermore, we have shown the effect of reaction medium on polymerization control wherein the deactivation may become poor/slow in

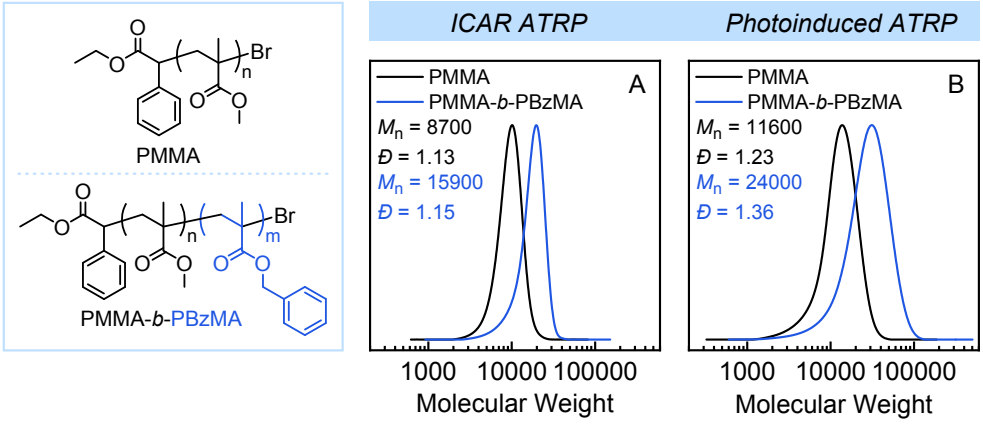

Figure 4. Chain extension experiments of PMMA with BzMA under (A) ICAR and (B) photoinduced ATRP conditions.

polar media yielding polymers with large dispersity. The results of this work provide further understanding of iron-catalyzed ATRP and show that a delicate balance of all ATRP components, including initiator, catalyst, and reaction medium is needed for performing well-controlled polymerizations. Ultimately, the $FeBr_3$/TBABr system in anisole provided excellent polymerization control. Considering the great potential of iron catalysts in ATRP, future studies should expand upon mechanistic understanding of these systems as well as their utility in a wide range of monomers and reaction media.

Conflicts of interest

There are no conflicts to declare.

Acknowledgements

Financial support by the National Science Foundation (NSF, CHE 2000391 and 210891) is gratefully acknowledged. This paper is dedicated to Professor Yusuf Yagci on the occasion of his 70th birthday.

References

1. N. Corrigan, K. Jung, G. Moad, C. J. Hawker, K. Matyjaszewski and C. Boyer, *Prog. Polym. Sci.*, 2020, **111**, 101311.
2. K. Parkatzidis, H. S. Wang, N. P. Truong and A. Anastasaki, *Chem*, 2020, **6**, 1575-1588.
3. J.-S. Wang and K. Matyjaszewski, *J. Am. Chem. Soc.*, 1995, **117**, 5614-5615.
4. K. Matyjaszewski and J. Xia, *Chem. Rev.*, 2001, **101**, 2921-2990.
5. K. Matyjaszewski, *Macromolecules*, 2012, **45**, 4015-4039.
6. S. Perrier, *Macromolecules*, 2017, **50**, 7433-7447.
7. J. Chiefari, Y. K. Chong, F. Ercole, J. Krstina, J. Jeffery, T. P. T. Le, R. T. A. Mayadunne, G. F. Meijs, C. L. Moad, G. Moad, E. Rizzardo and S. H. Thang, *Macromolecules*, 1998, **31**, 5559-5562.
8. J. Nicolas, Y. Guillaneuf, C. Lefay, D. Bertin, D. Gigmes and B. Charleux, *Prog. Polym. Sci.*, 2013, **38**, 63-235.
9. T. G. Ribelli, F. Lorandi, M. Fantin and K. Matyjaszewski, *Macromol. Rapid Commun.*, 2019, **40**, 1800616.
10. W. Tang and K. Matyjaszewski, *Macromolecules*, 2007, **40**, 1858-1863.
11. S. Lanzalaco, M. Fantin, O. Scialdone, A. Galia, A. A. Isse, A. Gennaro and K. Matyjaszewski, *Macromolecules*, 2017, **50**, 192-202.
12. S. Dadashi-Silab, G. Szczepaniak, S. Lathwal and K. Matyjaszewski, *Polym. Chem.*, 2020, **11**, 843-848.
13. C.-G. Wang, A. M. L. Chong, H. M. Pan, J. Sarkar, X. T. Tay and A. Goto, *Polym. Chem.*, 2020, **11**, 5559-5571.
14. I. Onishi, K.-Y. Baek, Y. Kotani, M. Kamigaito and M. Sawamoto, *J. Polym. Sci., Part A: Polym. Chem.*, 2002, **40**, 2033-2043.
15. Z.-H. Chen, Y. Ma, X.-Y. Wang, X.-L. Sun, J.-F. Li, B.-H. Zhu and Y. Tang, *ACS Cat.*, 2020, **10**, 14127-14134.
16. K. Matyjaszewski, S. Gaynor and J.-S. Wang, *Macromolecules*, 1995, **28**, 2093-2095.
17. K. Parkatzidis, M. Rolland, N. P. Truong and A. Anastasaki, *Polym. Chem.*, 2021, **12**, 5583-5588.
18. R. Poli, L. E. N. Allan and M. P. Shaver, *Prog. Polym. Sci.*, 2014, **39**, 1827-1845.
19. Z. Xue, D. He and X. Xie, *Polym. Chem.*, 2015, **6**, 1660-1687.
20. S. Dadashi-Silab and K. Matyjaszewski, *Molecules*, 2020, **25**, 1648.
21. A. Simakova, M. Mackenzie, S. E. Averick, S. Park and K. Matyjaszewski, *Angew. Chem. Int. Ed.*, 2013, **52**, 12148-12151.
22. S. J. Sigg, F. Seidi, K. Renggli, T. B. Silva, G. Kali and N. Bruns, *Macromol. Rapid Commun.*, 2011, **32**, 1710-1715.
23. Z. Xue, N. T. B. Linh, S. K. Noh and W. S. Lyoo, *Angew. Chem. Int. Ed.*, 2008, **47**, 6426-6429.
24. K. Nishizawa, M. Ouchi and M. Sawamoto, *Macromolecules*, 2013, **46**, 3342-3349.
25. Y. Wang, Y. Kwak and K. Matyjaszewski, *Macromolecules*, 2012, **45**, 5911-5915.
26. M. Y. Khan, J. Zhou, X. Chen, A. Khan, H. Mudassir, Z. Xue, S. W. Lee and S. K. Noh, *Polymer*, 2016, **90**, 309-316.
27. T. Ando, M. Kamigaito and M. Sawamoto, *Macromolecules*, 1997, **30**, 4507-4510.
28. K. Matyjaszewski, M. Wei, J. Xia and N. E. McDermott, *Macromolecules*, 1997, **30**, 8161-8164.
29. H. Schroeder, K. Matyjaszewski and M. Buback, *Macromolecules*, 2015, **48**, 4431-4437.
30. V. C. Gibson, R. K. O'Reilly, W. Reed, D. F. Wass, A. J. P. White and D. J. Williams, *Chem. Commun.*, 2002, DOI: 10.1039/B204510A, 1850-1851.
31. R. K. O'Reilly, M. P. Shaver, V. C. Gibson and A. J. P. White, *Macromolecules*, 2007, **40**, 7441-7452.
32. M. P. Shaver, L. E. N. Allan, H. S. Rzepa and V. C. Gibson, *Angew. Chem. Int. Ed.*, 2006, **45**, 1241-1244.
33. Y. Azuma, T. Terashima and M. Sawamoto, *ACS Macro Lett.*, 2017, **6**, 830-835.
34. L. E. N. Allan, J. P. MacDonald, G. S. Nichol and M. P. Shaver, *Macromolecules*, 2014, **47**, 1249-1257.
35. L. E. N. Allan, J. P. MacDonald, A. M. Reckling, C. M. Kozak and M. P. Shaver, *Macromol. Rapid Commun.*, 2012, **33**, 414-418.
36. H. Schroeder, B. R. M. Lake, S. Demeshko, M. P. Shaver and M. Buback, *Macromolecules*, 2015, **48**, 4329-4338.
37. M. Teodorescu, S. G. Gaynor and K. Matyjaszewski, *Macromolecules*, 2000, **33**, 2335-2339.
38. J. Wang, J. Han, X. Xie, Z. Xue, C. Fliedel and R. Poli, *Macromolecules*, 2019, **52**, 5366-5376.
39. M. Rolland, N. P. Truong, R. Whitfield and A. Anastasaki, *ACS Macro Lett.*, 2020, **9**, 459-463.
40. J. Wang, X. Xie, Z. Xue, C. Fliedel and R. Poli, *Polym. Chem.*, 2020, **11**, 1375-1385.
41. Y. Wang, Y. Zhang, B. Parker and K. Matyjaszewski, *Macromolecules*, 2011, **44**, 4022-4025.
42. S. Dadashi-Silab, X. Pan and K. Matyjaszewski, *Macromolecules*, 2017, **50**, 7967-7977.
43. S. Dadashi-Silab and K. Matyjaszewski, *ACS Macro Lett.*, 2019, **8**, 1110-1114.
44. K. Mukumoto, Y. Wang and K. Matyjaszewski, *ACS Macro Lett.*, 2012, **1**, 599-602.

45. M. Ishio, M. Katsube, M. Ouchi, M. Sawamoto and Y. Inoue, *Macromolecules*, 2009, **42**, 188-193.
46. H. Schroeder, J. Buback, S. Demeshko, K. Matyjaszewski, F. Meyer and M. Buback, *Macromolecules*, 2015, **48**, 1981-1990.
47. N. W. Gregory, *Inorg. Chem.*, 1983, **22**, 3750-3754.
48. M. R. Knecht and R. M. Crooks, *New J. Chem.*, 2007, **31**, 1349-1353.
49. Y. Wang and K. Matyjaszewski, *Macromolecules*, 2010, **43**, 4003-4005.
50. X. Pan, N. Malhotra, J. Zhang and K. Matyjaszewski, *Macromolecules*, 2015, **48**, 6948-6954.
51. X. Pan, N. Malhotra, S. Dadashi-Silab and K. Matyjaszewski, *Macromol. Rapid Commun.*, 2017, **38**, 1600651.
52. W. Tang, Y. Kwak, W. Braunecker, N. V. Tsarevsky, M. L. Coote and K. Matyjaszewski, *J. Am. Chem. Soc.*, 2008, **130**, 10702-10713.